Heliyon 10 (2024) e23659

Contents lists available at ScienceDirect

Heliyon

journal homepage: www.cell.com/heliyon

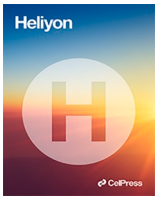

A novel sphingolipid metabolism-related long noncoding RNA signature predicts the prognosis, immune landscape and therapeutic response in pancreatic adenocarcinoma

Xiaolan He *, Zhengyang Xu, Ruiping Ren, Peng Wan, Yu Zhang, Liangliang Wang, Ying Han

Department of Chemoradiotherapy, The Affiliated People's Hospital of Ningbo University, Ningbo, China

ARTICLE INFO

Keywords:
Sphingolipid metabolism
Pancreatic adenocarcinoma
lncRNA
Prognosis
Tumor immune microenvironment
Tumor biomarker

ABSTRACT

Sphingolipid metabolism affects prognosis and resistance to immunotherapy in patients with cancer and is an emerging target in cancer therapy with promising diagnostic and prognostic value. Long noncoding ribonucleic acids (lncRNAs) broadly regulate tumour-associated metabolic reprogramming. However, the potential of sphingolipid metabolism-related lncRNAs in pancreatic adenocarcinoma (PAAD) is poorly understood. In this study, coexpression algorithms were employed to identify sphingolipid metabolism-related lncRNAs. The least absolute shrinkage and selection operator (LASSO) algorithm was used to develop a sphingolipid metabolism-related lncRNA signature (SMLs). The prognostic predictive stability of the SMLs was validated using Kaplan–Meier. Univariate and multivariate Cox, receiver operating characteristic (ROC) and clinical stratification analyses were used to comprehensively assess the SMLs. Gene set variation analysis (GSVE), gene ontology (GO) and tumor mutation burden (TMB) analysis explored the potential mechanisms. Additionally, single sample gene set enrichment analysis (ssGSEA), ESTIMATE, immune checkpoints and drug sensitivity analysis were used to investigate the potential predictive function of the SMLs. Finally, an SMLs-based consensus clustering algorithm was utilized to differentiate patients and determine the suitable population for immunotherapy. The results showed that the SMLs consists of seven sphingolipid metabolism-related lncRNAs, which can well determine the clinical outcome of individuals with PAAD, with high stability and general applicability. In addition, the SMLs-based consensus clustering algorithm divided the TCGA-PAAD cohort into two clusters, with Cluster 1 showing better survival than Cluster 2. Additionally, Cluster 1 had a higher level of immune cell infiltration than Cluster 2, which combined with the higher levels of immune checkpoints in Cluster 1 suggests that Cluster 1 is more consistent with an immune 'hot tumor' profile and may respond better to immune checkpoint inhibitors (ICIs). This study offers new insights regarding the potential role of sphingolipid metabolism-related lncRNAs as biomarkers in PAAD. The constructed SMLs and the SMLs-based clustering are valuable tools for predicting clinical outcomes in PAAD and provide a basis for clinical selection of individualized treatments.

* Corresponding author.
E-mail address: ab1249871192@163.com (X. He).

https://doi.org/10.1016/j.heliyon.2023.e23659
Received 26 March 2023; Received in revised form 23 November 2023; Accepted 9 December 2023
Available online 12 December 2023

1. Introduction

Pancreatic cancer is currently the seventh major cause of cancer-related deaths globally, and the mortality incidence rate and 5-year survival rate are similar at 9 %–11 %. Thus, pancreatic cancer significantly affects human life and health [1,2]. Pancreatic cancer is extremely malignant, and approximately 90 % of all pathological types are pancreatic adenocarcinoma (PAAD). A study covering multiple populations showed an increasing trend in the incidence and mortality of pancreatic cancer [3]. Similarly, another study comprising populations from European Union countries showed that by 2025, pancreatic cancer will be the third major cause of cancer-related death [4]. Additionally, owing to the insidious onset of PAAD and the atypical early symptoms, most patients have advanced or metastatic tumors at the time of diagnosis. Therefore, it is vital to identify excellent biomarkers that can accurately stratify individuals with PAAD and determine the prognosis and biological behavior of different patient subgroups.

Sphingolipids are key structural components of cell membranes and have a critical function in maintaining the fluidity and barrier capacity of the cell membrane [5,6]. Sphingolipid metabolism is involved in cell proliferation, growth, apoptosis, lysosomal homeostasis and other biological processes and plays an essential role in tumor cell invasion, metastasis and immune regulation [7–9]. Additionally, sphingolipid metabolism regulates the malignant biological behavior of tumors through complex cellular signaling pathways [10]. Recent studies have reported that sphingolipid metabolism can mediate the interaction between lysosomes and mitochondria, leading to significant cell death in pancreatic cancer cells and slowing tumor growth in vivo [11]. Moreover, ceramide-1-phosphate transfer protein has been demonstrated to promote the proliferation of pancreatic cancer cells via the sphingolipid metabolite ceramide and AKT signaling pathway [12]. Therefore, exploring the function of different signaling nodes in sphingolipid metabolism with respect to pancreatic cancer development is important for identifying and developing novel molecular targets and biomarkers.

With advances in genome sequencing, elucidating the vital role of long noncoding ribonucleic acids (lncRNAs) in cancer is a hot topic in the study of tumor pathogenesis. lncRNAs do not directly encode proteins but act as major regulators of gene regulation, exerting their biological functions through epigenetic, transcriptional and posttranscriptional regulation. lncRNAs are engaged in a diverse range of biological processes and regulate tumorigenesis, angiogenesis and immunomodulation [13–16]. Moreover, abnormal lncRNA expression and mutations have been shown to be closely related to tumor prognosis and drug resistance, emphasizing their use as novel biomarkers and potential therapeutic targets for cancer [17,18]. Additionally, there is growing evidence that lncRNAs are engaged in the regulation of tumor-related metabolic reprogramming, such as glucose, glutamine and lipid metabolism [19–22]. However, the regulatory functions and applications of sphingolipid metabolism-associated lncRNAs in PAAD remain unexplored.

Here, we aimed to construct a novel sphingolipid metabolism-related lncRNA signature (SMLs) that can predict the prognosis of individuals with PAAD, thereby providing a clinical basis for personalized treatment options. Furthermore, SMLs-based consensus clustering could aid in stratifying patients into different clusters, differentiating patients into distinct immune subsets and consequently facilitating the selection process of the choice of immunotherapy.

2. Materials and METHODS

2.1. Dataset selection

Transcriptome profiling, simple nucleotide variation (SNV) and clinicopathological parameters of individuals with PAAD were collected from the TCGA-PAAD cohort in the Cancer Genome Atlas (TCGA) repository (https://portal.gdc.cancer.gov/repository). Cases with both transcriptomic data and survival data were included in subsequent analyses. The Strawberry Perl programming language (version 5.32.1.1) was used to differentiate between lncRNAs and mRNAs in the TCGA-PAAD cohort and obtain a matrix of corresponding expression data for further profiling [23]. The 97 sphingolipid metabolism-related genes (Table S1) included in the present research were acquired from the InnateDB portal (http://www.innatedb.com) [24,25].

2.2. Determination of sphingolipid metabolism-related lncRNAs

The R package ‘limma’ was utilized to obtain the mRNA data matrix of 97 sphingolipid metabolism-related genes in the TCGA-PAAD cohort [26]. The lncRNAs associated with sphingolipid metabolism-related mRNAs were derived using a coexpression algorithm (Pearson coefficient >0.4, $p < 0.001$) and determined to be sphingolipid metabolism-related lncRNAs [27]. The package ‘igraph’ was employed to map the relationship network of sphingolipid metabolism-related genes and lncRNAs.

2.3. Construction of SMLs in PAAD

First, the TCGA-PAAD cohort was randomly divided into a training set and a testing set at a 1:1 ratio. Subsequently, univariate Cox (uni-Cox) regression algorithms were utilized to identify sphingolipid metabolism-related lncRNAs associated with survival in the training set ($p < 0.05$), and prognostic forest maps and expression heatmaps were drawn using the ‘survival’ and ‘pheatmap’ packages. To avoid overfitting, the Least Absolute Shrinkage and Selection Operator (LASSO) algorithm determined the optimal sphingolipid metabolism-associated lncRNAs that can be used in the development of the SMLs [28]. The ‘caret’ and ‘glmnet’ packages were utilized in the construction of the SMLs. The correlations between lncRNAs and sphingolipid metabolism-related genes were analyzed, and correlation heatmaps were plotted via the ‘ggplot2’, ‘ggExtra’ and ‘tidyverse’ packages. Finally, the risk score for each PAAD individual

was derived using the following equation: SMLs (Risk score) $= \sum_{i+1}^{n} \beta(i) * \chi(i)$, where β represents the risk correlation coefficient of a lncRNA in the SMLs, and χ represents the expression of the corresponding lncRNA. Based on the median score of the training set, all individuals in the TCGA-PAAD cohort were classified into high- and low-risk groups.

2.4. Validation of the SMLs in PAAD

To verify the predictive power of the developed SMLs in the clinical outcomes of PAAD, we first conducted separate survival analyses for the training, testing and TCGA-PAAD sets and visualized the results by plotting Kaplan–Meier (K−M) curves, risk heatmaps and survival status maps using the 'survminer' and 'survivor' packages [29]. Additionally, uni-Cox and multivariate Cox (multi-Cox) analyses determined whether the SMLs-based risk score was an independent predictor of clinical prognosis. Finally, time-dependent receiver operating characteristic (ROC) curves were plotted to validate the accuracy of the SMLs in predicting patient survival, with different clinical phenotypes (age, sex, grade and stage) used as variables for comparison, using 'timeROC', 'survminer' and 'survivor' packages.

2.5. Correlation of the SMLs with clinicopathological phenotypes in PAAD

To verify the stability and adaptability of the SMLs in PAAD, we analyzed the survival differences between the two risk subgroups based on the clinicopathological subgroups (sex, age, grade and stage), and the 'survminer' and 'survival' packages were conducted to draw the K−M curves. Finally, the 'ComplexHeatmap' package was utilized to draw the correlation bar chart of the different clinical phenotypes in the two groups [30].

2.6. Functional exploration based on the SMLs

To explore differences in biological function between the two risk subgroups, the Gene Set Variance Analysis (GSVA) algorithm was initially used to obtain enrichment of the Kyoto Encyclopedia of Genes and Genomes (KEGG) pathways in the risk subgroups [31]. The relationship between the KEGG pathway and lncRNA expression in the SMLs was further analyzed using the packages 'GSVA', 'GSEABase', 'reshape2' and 'limma' and visualized using 'pheatmap' and 'ggplot2'. Additionally, we explored the enrichment of differentially expressed genes (DEGs) between the risk subgroups in terms of cellular component, molecular function and biological processes via Gene Ontology (GO) analysis, which utilized the 'DOSE', 'clusterProfiler' and 'org.Hs.eg.db' packages. Furthermore, 'ggplot2', 'ComplexHeatmap', 'RColorBrewer', 'ggpubr' and 'circlize' were used to visualize the enrichment results.

2.7. Correlation analysis of the SMLs and tumor mutation burden (TMB)

Numerous studies have demonstrated that TMB and mutation-associated neoantigens are closely related, and TMB is also considered a biomarker that predicts the efficiency of immunotherapy in some tumors [32]. The downloaded SNV data of the TCGA-PAAD cohort were transformed using Perl scripts to retrieve the TMB matrix for every sample and the mutation matrix for each gene. The 25 most frequently mutated genes in the TCGA-PAAD cohort were further extracted and the 'maftools' package was utilized to map the mutation waterfall plot for these 25 genes in the two risk groups. Additionally, TMB differences between the risk subgroups were further analyzed, and the 'ggpubr' package was utilized to visualize the violin plots of the differential results. Finally, survival differences between patients in different TMB subgroups combined with patients in different risk subgroups were analyzed and K−M survival curves were plotted.

2.8. Analysis of the tumor immune microenvironment (TIME) and immunotherapy

To explore the association between the TIME and SMLs in PAAD, we first extracted the tumor infiltrating immune cell file from the TIMER2.0 platform (http://timer.comp-genomics.org/), which contains the TCGA immune cell infiltration data calculated by the EPIC, TIMER, XCELL, CIBERSORT, QUANTISEQ, CIBERSORT-ABS and MCPCOUNTER platforms [33]. Spearman's correlation algorithm was subsequently performed to obtain correlation coefficients between risk scores and tumor-infiltrating immune cells. Following this, the 'ggtext', 'ggpubr', 'ggplot2', 'scales' and 'tidyverse' packages were utilized to plot correlation bubble plots.

Gene set enrichment analysis (GSEA) enables the enrichment analysis of gene sets with physiological regulatory roles and biological effects [34,35]. Single sample GSEA (ssGSEA) was performed utilizing 'GSEABase' and 'GSVA' to quantify the degree of infiltration of different immune cells in the TCGA-PAAD cohort, consequently obtaining the corresponding scores of immune cells and immune functions. Then, the differences in immune cell score and function score in the high- and low-risk subgroups were analyzed utilizing the 'GSEABase' and 'GSVA' packages, and 'reshape2', 'pheatmap', and 'ggpubr' were employed to plot boxplots of the results.

Estimation of STromal and Immune cells in MAlignant Tumor tissues using Expression data (ESTIMATE) analysis is an expression-based tumor purity determination algorithm [36]. Here, the 'ESTIMATE' algorithm was utilized to quantify the number of immune cells and stromal cells in the TCGA-PAAD samples, thereby obtaining the corresponding immune cell and stromal cell scores. The total of these two scores is the ESTIMATE score. Then, we analyzed the difference in the different types of scores between the two risk populations and drew difference boxplots using the 'ggpubr' package.

Immune checkpoints are inhibitory regulatory molecules in the immune system. Their expression on immune cells will inhibit

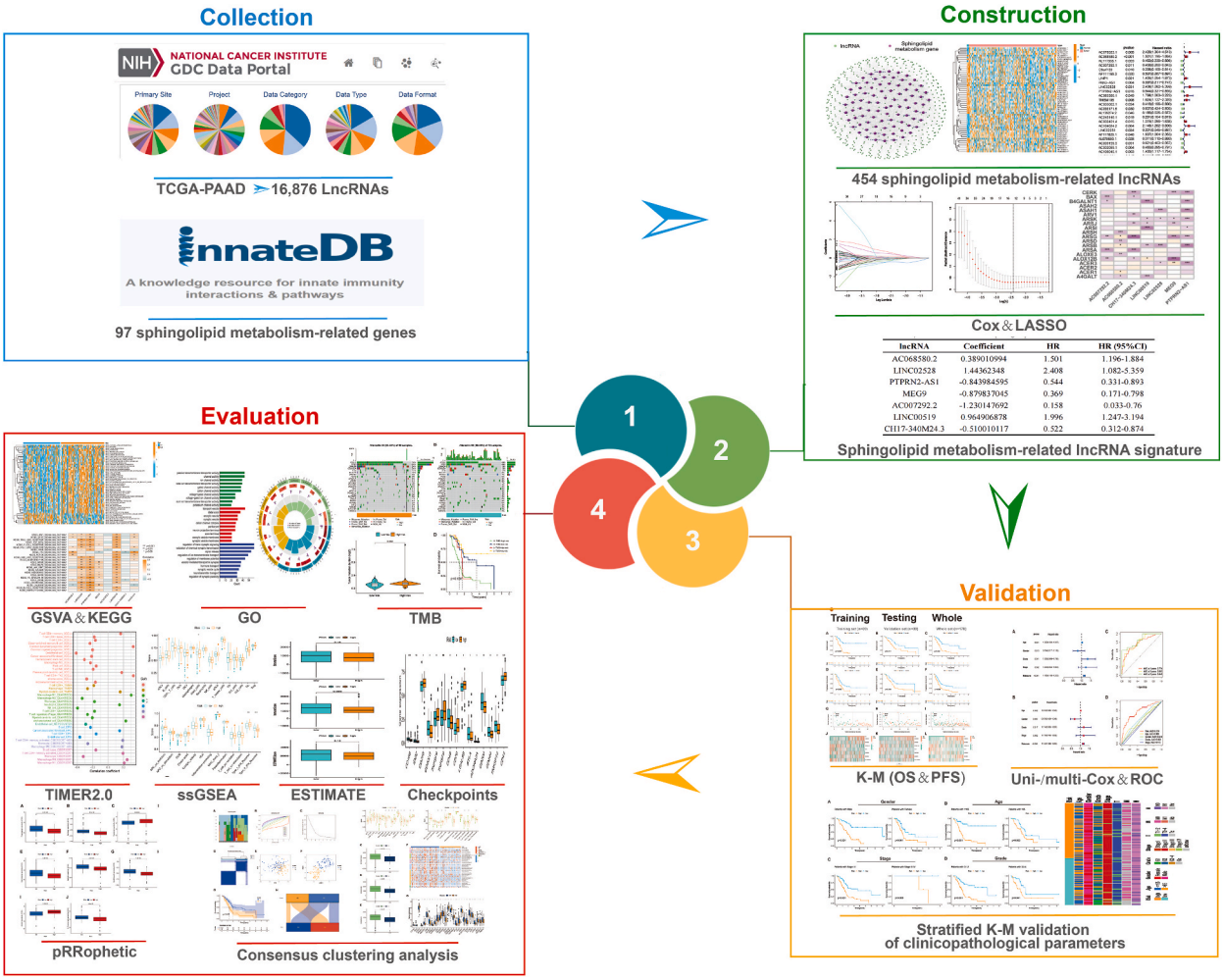

Fig. 1. Flowchart of the study.

immune cell function, preventing the body from producing an effective antitumour immune response and promoting tumor immune escape [37]. Here, we thus analyzed the differences in the mRNA expression of immune checkpoints in the different risk subgroups.

2.9. Drug sensitivity analysis

To evaluate the use of the SMLs in the individualized clinical management of PAAD, we utilized the 'pRRophetic' to compare the differences in the half-maximal inhibitory concentrations (IC50) of 138 chemotherapeutic agents and targeted drugs in the two risk populations [38]. The difference in IC50 was represented using boxplots ($p < 0.001$).

2.10. Consensus clustering analysis

It has been shown that molecular typing based on consensus clustering analysis can identify tumor subgroups with distinct TIME characteristics and may influence the efficacy of immunotherapy [39,40]. An SMLs-based consensus clustering analysis was conducted utilizing the 'ConsensusClusterPlus' package to classify all individuals into different clusters [41]. Principal component analysis (PCA) was conducted on the different clusters using the 'ggplot2' and 'Rtsne' packages. Additionally, survival differences between patients in different clusters were analyzed and visualized using K–M curves. Finally, ssGSEA, ESTIMATE and immune checkpoints were also analyzed in the different clusters.

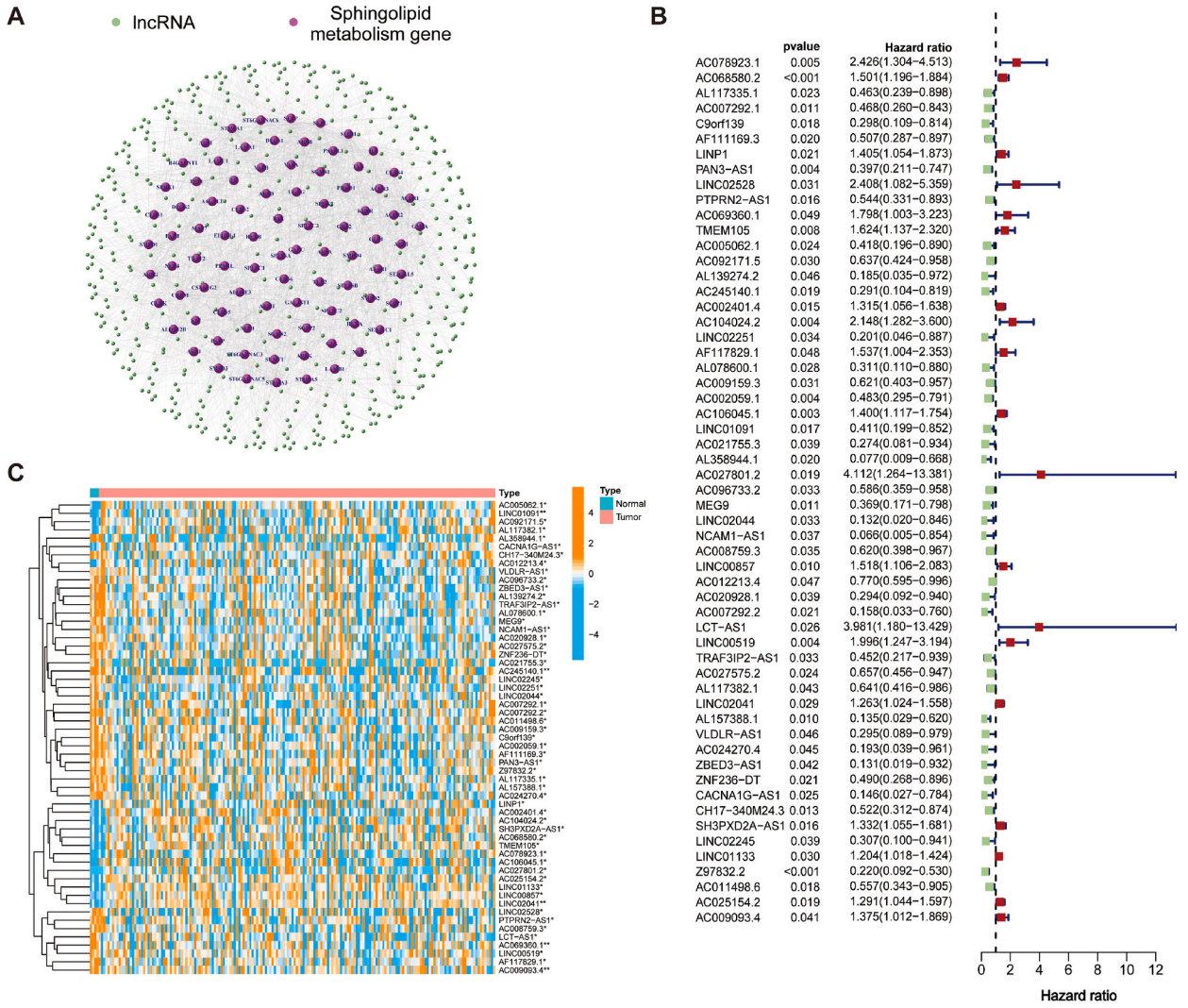

Fig. 2. Identification of sphingolipid metabolism-related lncRNAs. (A) Network relationship map of the 454 sphingolipid metabolism-associated lncRNAs and sphingolipid metabolism-associated genes. **(B)** Forest plot of the 57 sphingolipid metabolism-related lncRNAs associated with survival. **(C)** Expression heat map of the 57 sphingolipid metabolism-related lncRNAs.

3. Results

3.1. Acquisition of sphingolipid metabolism-related lncRNAs

Fig. 1 presents the design of this study. The processing transcriptome data from the TCGA-PAAD cohort identified 16,876 lncRNAs. A total of 97 sphingolipid metabolism-related genes were extracted from the InnateDB database, and 454 lncRNAs were identified as sphingolipid metabolism-related lncRNAs based on the coexpression algorithm (Fig. 2A).

3.2. Construction of the SMLs

The TCGA-PAAD cohort was randomly divided into training and testing cohorts, and the clinicopathological parameters of the individuals in the two cohorts are shown in Table 1. Cox regression identified 57 sphingolipid metabolism-related lncRNAs associated with survival ($p < 0.05$) (Fig. 2B). Survival-related lncRNAs have different expression statuses in PAAD tumor and normal samples (Fig. 2C). To fit the generalized linear model while performing variable screening and complexity adjustment, LASSO regression was performed (Fig. 3A and B), identifying seven lncRNAs for use in the signature construction (Fig. 3C). Risk scores were generated for each sample based on the risk coefficients corresponding to the seven lncRNAs (Table 2). SMLs (Risk score) = (0.389010994 × AC068580.2) + (1.44362348 × LINC02528) + (−0.843984595 × PTPRN2-AS1) + (−0.879837045 × MEG9) + (−1.230147692 × AC007292.2) + (0.964906878 × LINC00519) + (−0.510010117 × CH17-340M24.3). The expression of the seven lncRNAs correlated

Table 1
The clinicopathological features in different cohorts.

Clinicopathological Features	Stratification	Total set (n = 178)	Training set (n = 89)	Testing set (n = 89)	*p*-value
Age	≤65	94 (52.81 %)	48 (53.93 %)	46 (51.69 %)	0.8807
	>65	84 (47.19 %)	41 (46.07 %)	43 (48.31 %)	
Gender	Female	80 (44.94 %)	35 (39.33 %)	45 (50.56 %)	0.1751
	Male	98 (55.06 %)	54 (60.67 %)	44 (49.44 %)	
Grade	G1	31 (17.42 %)	13 (14.61 %)	18 (20.22 %)	0.126
	G2	95 (53.37 %)	43 (48.31 %)	52 (58.43 %)	
	G3	48 (26.97 %)	29 (32.58 %)	19 (21.35 %)	
	G4	2 (1.12 %)	2 (2.25 %)	0 (0 %)	
	Unknown	2 (1.12 %)	2 (2.25 %)	0 (0 %)	
TNM Stage	Stage I	21 (11.8 %)	11 (12.36 %)	10 (11.24 %)	0.9439
	Stage II	147 (82.58 %)	73 (82.02 %)	74 (83.15 %)	
	Stage III	3 (1.69 %)	1 (1.12 %)	2 (2.25 %)	
	Stage IV	4 (2.25 %)	2 (2.25 %)	2 (2.25 %)	
	Unknown	3 (1.69 %)	2 (2.25 %)	1 (1.12 %)	
T Stage	T1	7 (3.93 %)	3 (3.37 %)	4 (4.49 %)	0.8853
	T2	24 (13.48 %)	11 (12.36 %)	13 (14.61 %)	
	T3	142 (79.78 %)	72 (80.9 %)	70 (78.65 %)	
	T4	3 (1.69 %)	1 (1.12 %)	2 (2.25 %)	
	Unknown	2 (1.12 %)	2 (2.25 %)	0 (0 %)	
N Stage	N0	49 (27.53 %)	28 (31.46 %)	21 (23.6 %)	0.2477
	N1	124 (69.66 %)	57 (64.04 %)	67 (75.28 %)	
	Unknown	5 (2.81 %)	4 (4.49 %)	1 (1.12 %)	
M Stage	M0	80 (44.94 %)	41 (46.07 %)	39 (43.82 %)	1
	M1	4 (2.25 %)	2 (2.25 %)	2 (2.25 %)	
	Unknown	94 (52.81 %)	46 (51.69 %)	48 (53.93 %)	

strongly with the expression of sphingolipid metabolism-related genes (Fig. 3D).

3.3. Validation of the SMLs

To validate the prognostic prediction power of the SMLs, we first performed a survival analysis. K–M curves for overall survival (OS) and progression-free survival (PFS) revealed that high-risk groups in the training, testing and TCGA-PAAD sets had a worse prognosis than the low-risk groups (Fig. 4A–F). Survival status plots showed an increase in the number of patients with mortality status as their risk score increased (Fig. 4G–I). These findings highlight the stability and reliability of the SMLs. Additionally, the lncRNA expression heatmaps in the three cohorts showed that AC068580.2, LINC02528 and LINC00519 were highly expressed in the high-risk subgroup, while PTPRN2-AS1, MEG9, AC007292.2 and CH17-340M24.3 were highly expressed in the low-risk subgroup (Fig. 4J-L).

3.4. Assessment of the SMLs

Cox regression analysis revealed that the SMLs was an independent variable affecting the clinical outcomes of patients with PAAD. The hazard ratios for the risk scores in Uni- and multi-Cox regression were 1.153 and 1.149 ($p < 0.001$), respectively (Fig. 5A and B). Additionally, the ROC curves showed that the SMLs had area under the curve (AUC) values of 0.774, 0.800 and 0.848 at 1-, 3- and 5-year, respectively (Fig. 5C). The AUC values for the SMLs were greater than those for other clinicopathological features (age, sex, grade and stage) (Fig. 5D), indicating the predictive reliability of the SMLs. Finally, we also assessed the predictive power of the SMLs across different clinicopathological characteristics, including patient sex, age, stage and grade. K–M curves showed that survival was significantly worse in high-risk patients across age, gender and tumour grade subgroups (Fig. 6A–D). Although there was no significant difference in survival between the risk groups in individuals with stage III-IV ($p = 0.055$), a trend towards separate K-M curves was observed, which could be attributed to the smaller number of cases with stage III-IV (only three patients in stage III and four patients in stage IV). Thus, the above results suggest that the constructed SMLs has high stability and adaptability. Finally, the status of the clinical parameters of patients in the different risk groups is shown by heatmaps (Fig. 6E).

3.5. GSVA and GO analysis

To investigate the characteristics of biological behavior in populations stratified by risk using the SMLs, GSVA was performed to analyze the enrichment of the KEGG pathway between the risk groups. The outcomes showed that pancreatic cancer, DNA replication, mismatch repair, nucleotide excision repair, steroid biosynthesis, pyrimidine metabolism, glutathione metabolism, porphyrin and chlorophyll metabolism, fructose and mannose metabolism, pentose phosphate pathway and glycolytic gluconeogenesis were enriched in the high-risk population. In contrast, in the low-risk population, the enriched pathways included primary bile acid biosynthesis, glycolipid biosynthesis and neuroactive ligand-receptor interactions (Fig. 7A). Additionally, further analysis revealed strong correlations between the expression of the seven lncRNAs in the SMLs and multiple signaling pathways including those of WNT, VEGF, mTOR, MAPK, JAK-STAT and TGF-β (Fig. 7B).

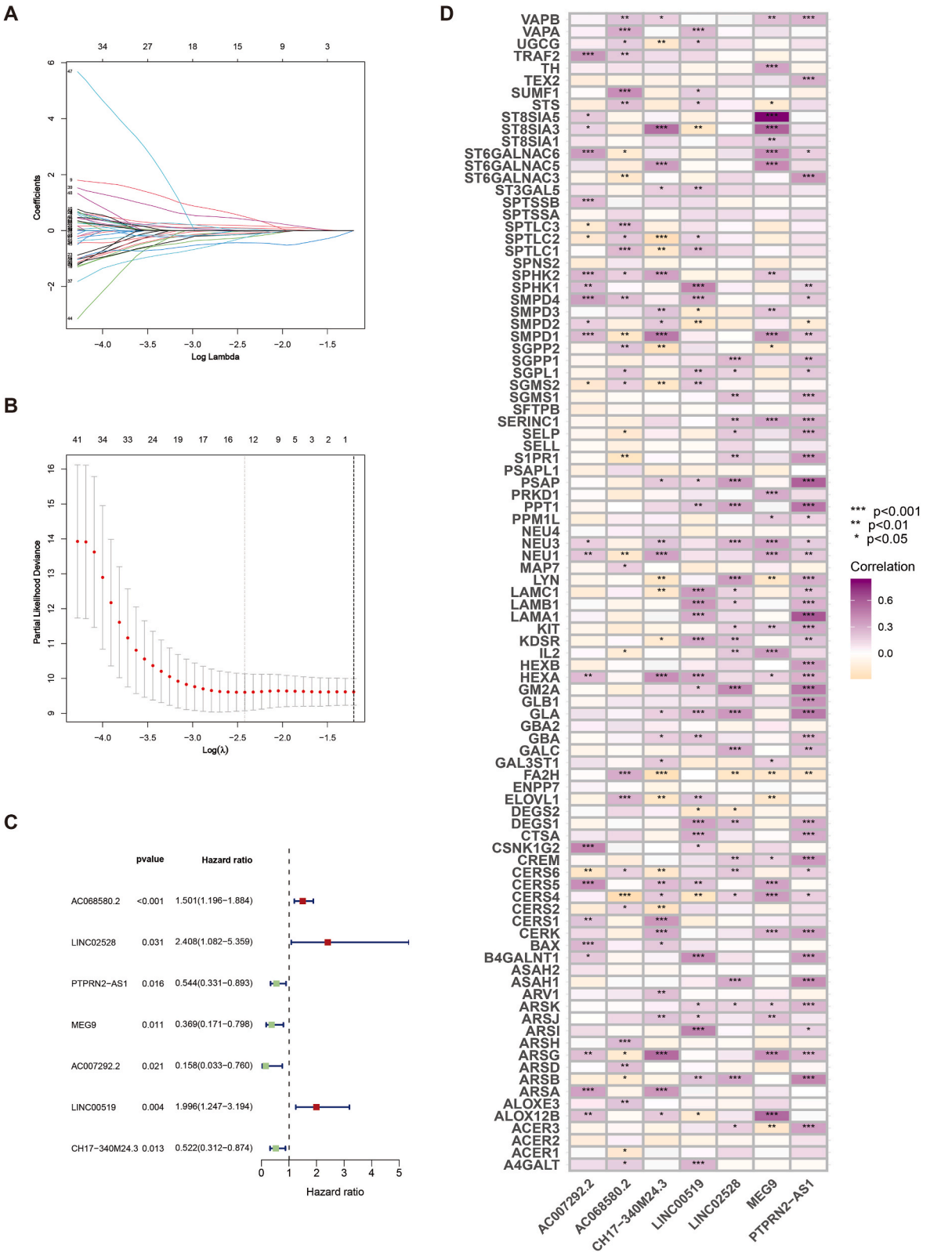

(caption on next page)

Fig. 3. Development of a sphingolipid metabolism-related signature. (A) LASSO coefficient curves for prognostic sphingolipid metabolism-related lncRNAs. **(B)** The vertical black line in the figure denotes the ideal log λ value. **(C)** Forest plot of the sphingolipid metabolism-related lncRNAs in the signature. **(D)** Heatmap showing the coexpression relationship between the sphingolipid metabolism-related signature and sphingolipid metabolism-related genes.

Table 2
| Risk coefficients for sphingolipid metabolism-related lncRNAs in the SMLs.

lncRNA	Coefficient	Hazard ratio	Hazard ratio (95%CI)	*p*-value
AC068580.2	0.389010994	1.501	1.196–1.884	<0.001
LINC02528	1.44362348	2.408	1.082–5.359	0.031
PTPRN2-AS1	−0.843984595	0.544	0.331–0.893	0.016
MEG9	−0.879837045	0.369	0.171–0.798	0.011
AC007292.2	−1.230147692	0.158	0.033–0.76	0.021
LINC00519	0.964906878	1.996	1.247–3.194	0.004
CH17-340M24.3	−0.510010117	0.522	0.312–0.874	0.013

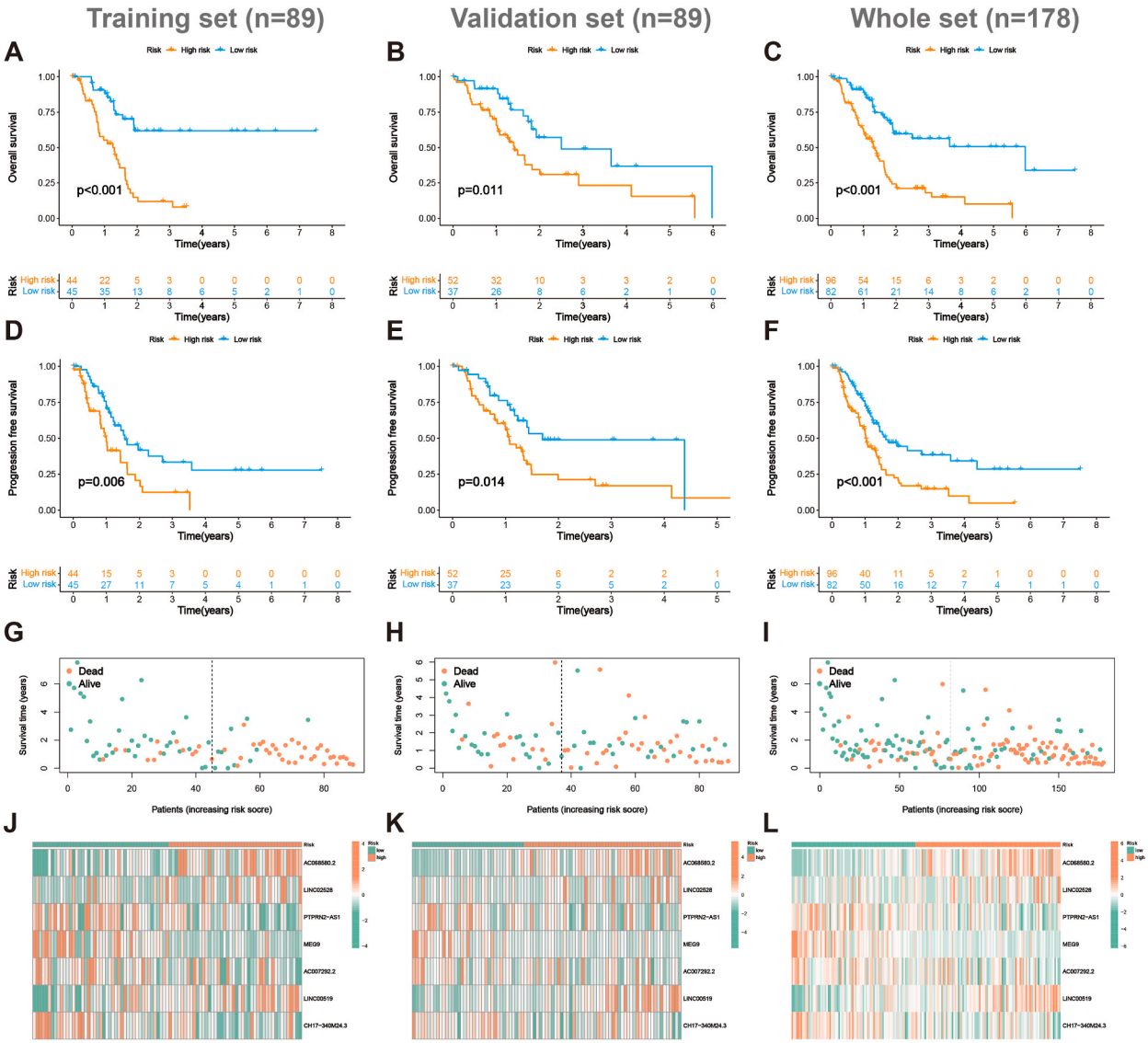

Fig. 4. Validation of the sphingolipid metabolism-related signature. (A–C) Kaplan–Meier curves of OS. **(D–F)** Kaplan–Meier curves of PFS. **(G–I)** Survival status of the individuals with PAAD in the three cohorts. **(J–L)** Heatmaps of the expression of the seven sphingolipid metabolism-related lncRNAs in the three sets.

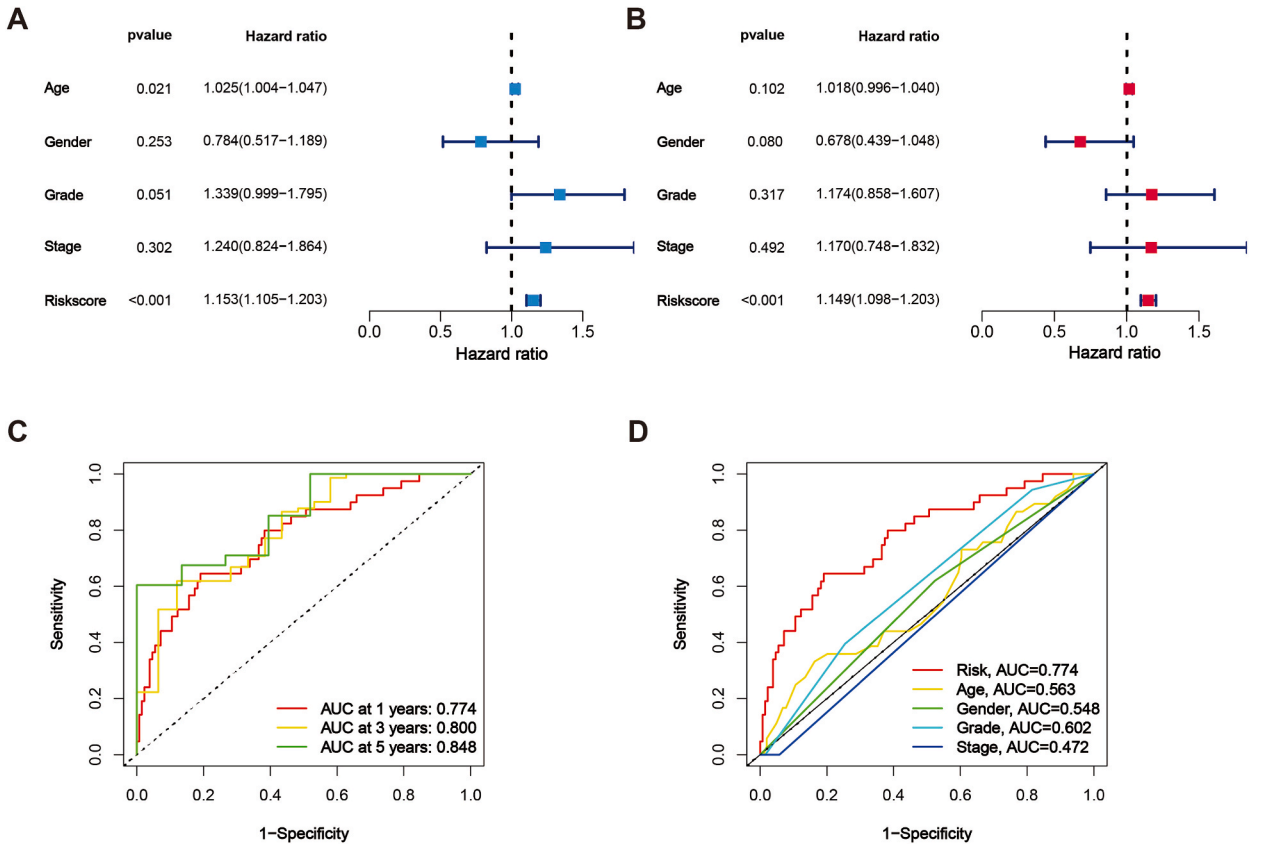

Fig. 5. Predictive performance of the sphingolipid metabolism-related signature. (A–B) Forest plot for univariate **(A)** and multivariate **(B)** Cox regression. **(C)** Time-independent ROC curves of the sphingolipid metabolism-related signature in the TCGA-PAAD cohort. **(D)** ROC curves for the risk score and clinicopathological parameters in the TCGA-PAAD cohort.

We further explored the molecular functions of the DEGs between different risk groups, their cellular environment and the biological processes in which they are involved. GO analysis indicated that the DEGs were enriched in biological processes such as the regulation of transsynaptic signaling, regulation of chemical synaptic transmission, signal release and regulation of ion transport. In terms of the cellular component, the enrichment sites included a transport vessel, distal axon, exogenic vessel and synaptic vessel. Finally, in terms of the molecular function, the enriched functions included passive transmission transmitter activity, channel activity, ion channel activity and metal transmission transmitter activity (Fig. 7C and D).

3.6. Correlation of the SMLs with TMB

Mutation waterfall plots revealed that the frequency of mutations in the high- and low-risk groups was 93.33 % and 69.44 %, respectively (Fig. 8A and B). Additionally, higher TMB levels were observed in the high-risk population ($p = 0.002$) (Fig. 8C). Furthermore, survival analysis of the high- and low-risk subgroups and the combination of high- and low-TMB subgroups showed significant differences in survival between the different subgroup combinations ($p < 0.001$). The worst OS was observed in the high-TMB/high-risk subgroup and the best OS was observed in the low-TMB/low-risk subgroup (Fig. 8D). Therefore, the signature combined with TMB levels could better predict the clinical outcomes of individuals with PAAD.

3.7. Correlation of the SMLs with TIME

Bubble plots from Spearman's correlation analysis showed that $CD8^+$ T cells were negatively correlated with risk scores in the XCELL and QUANTISEQ platforms. $CD4^+$ T cells were negatively correlated with risk scores in the EPIC and TIMER platforms. Additionally, M1 macrophages were positively correlated with risk scores in QUANTISEQ and XCELL platforms. However, the correlation of cancer-associated fibroblast with risk scores in XCELL and EPIC showed opposite results with coefficients of −0.21 and 0.15, respectively (Fig. 9A). However, ssGSEA revealed that only mast cells differed between the risk groups (Fig. 9B). Furthermore, ssGSEA outcomes also revealed no significant differences in most immune-related functions between the two risk subgroups, except for IFN response and MHC class I (Fig. 9C). This suggests that the SMLs-based risk stratification does not distinguish between the different TIME subtypes of PAAD. This was further validated by ESTIMATE analysis, wherein no significant differences in ESTIMATE, immune

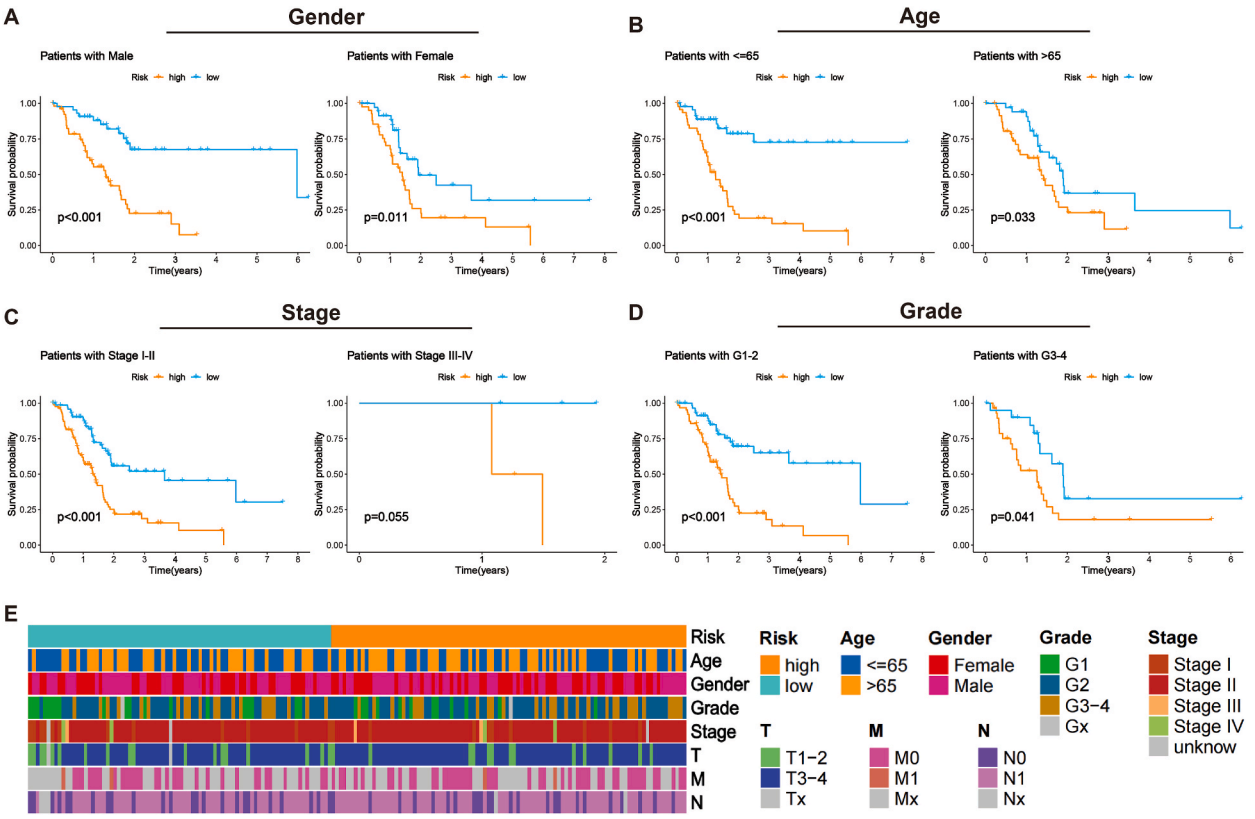

Fig. 6. Stratified Kaplan–Meier validation of clinicopathological parameters. (A–D) Kaplan–Meier curves stratified by sex **(A)**, age **(B)**, stage **(C)** and grade **(D)**. **(E)** Heatmap of the distribution of clinicopathological variables in subgroups.

and stromal scores were observed between the different risk groups (Fig. 9D–F). Furthermore, while some of the immune detection sites such as CD276, CD244, CD44 and LGALS9 differed between the two risk subgroups (Fig. 9G), the key targets of immune checkpoint inhibitors (ICIs), namely PD-1, PD-L1 and CTLA-4, were not differentially expressed in the risk groups.

3.8. Predicting drug sensitivity using the SMLs

Drug sensitivity analysis based on the pRRophetic algorithm revealed that the IC50 of some clinical chemotherapeutic agents and targeted therapeutics differed between the risk subgroups ($p < 0.001$) (Fig. 10A–J). Thapsigargin, paclitaxel, methotrexate, gemcitabine, gefitinib, epothilone B, doxorubicin and 5-fluorouracil had lower IC50s in the high-risk population while those of navitoclax and axitinib were higher.

3.9. Consensus clustering analysis based on the SMLs

Consensus clustering analysis based on the SMLs was performed to explore the characteristics of individuals with different molecular subtypes of PAAD. According to the cumulative distribution function (CDF) values, we divided the TCGA-PAAD cohort into two clusters (k = 2, Fig. 11A–D). PCA and tSNE significantly distinguished between the distribution characteristics of Cluster 1 and Cluster 2 (Fig. 11E and F). The K–M curve showed that survival was better in Cluster 1 than in Cluster 2 ($p < 0.001$) (Fig. 11G). The Sankey diagram showed that the majority of individuals in Cluster 1 were in the low-risk population, while the majority in Cluster 2 were in the high-risk population (Fig. 11H).

We further analyzed the TIME characteristics of the different clusters. The ssGSEA results revealed significantly higher infiltration levels of B cells, $CD8^+$ T cells, mast cells, neutrophils, natural killer cells, plasmacytoid dendritic cells, helper T cells, follicular helper T cells, Th1 cells, tumor-infiltrating lymphocytes and regulatory T cells in Cluster 1 (Fig. 12A). In terms of immune function, the pathways of cytokine–cytokine receptor, immune checkpoint, cytolytic activity, inflammation-promoting, T cell co-inhibition, T cell co-stimulation and Type II IFN response were significantly stronger in Cluster 1 (Fig. 12B). The ESTIMATE analysis similarly validated this finding, with Cluster 1 showing significantly higher ESTIMATE, immune and stromal scores than Cluster 2 (Fig. 12C–E). The heatmap of immune cell infiltration status revealed that the majority of immune cells had higher levels of infiltration in Cluster 1 (Fig. 12F). Furthermore, the differential analysis of immune checkpoints indicated that most of the immune checkpoints, including PD-1, LAG3, CD27 and CD48, were highly expressed in Cluster 1 compared to Cluster 2, which corroborated the outcomes of ssGSEA

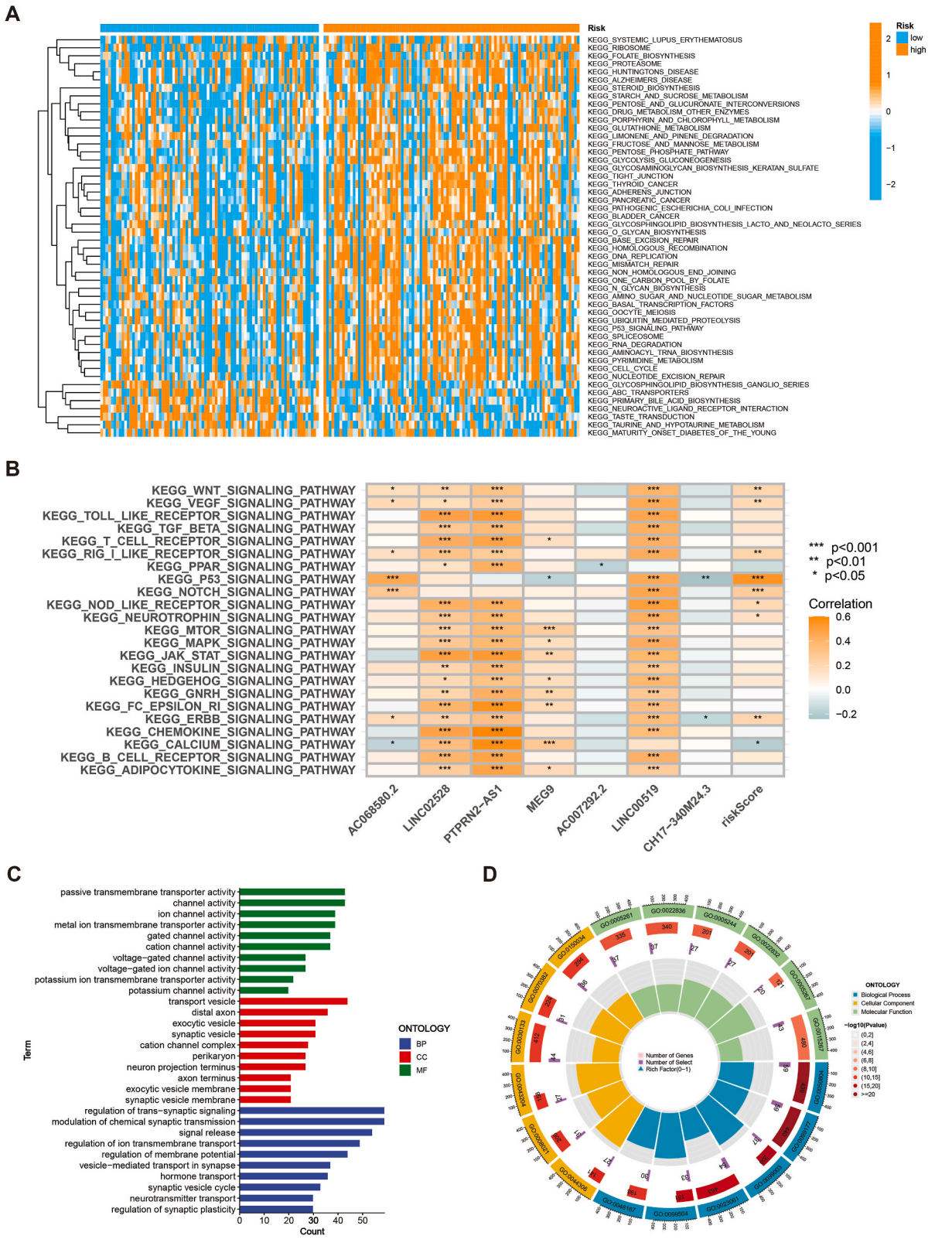

Fig. 7. Functional and pathway enrichment. (A) GSVA shows the enrichment of pathways for DEGs between the high- and low-risk subgroups. **(B)** Heatmap of the relationship between the KEGG pathways and the expression of signature-associated lncRNAs. **(C–D)** GO enrichment analysis of DEGs.

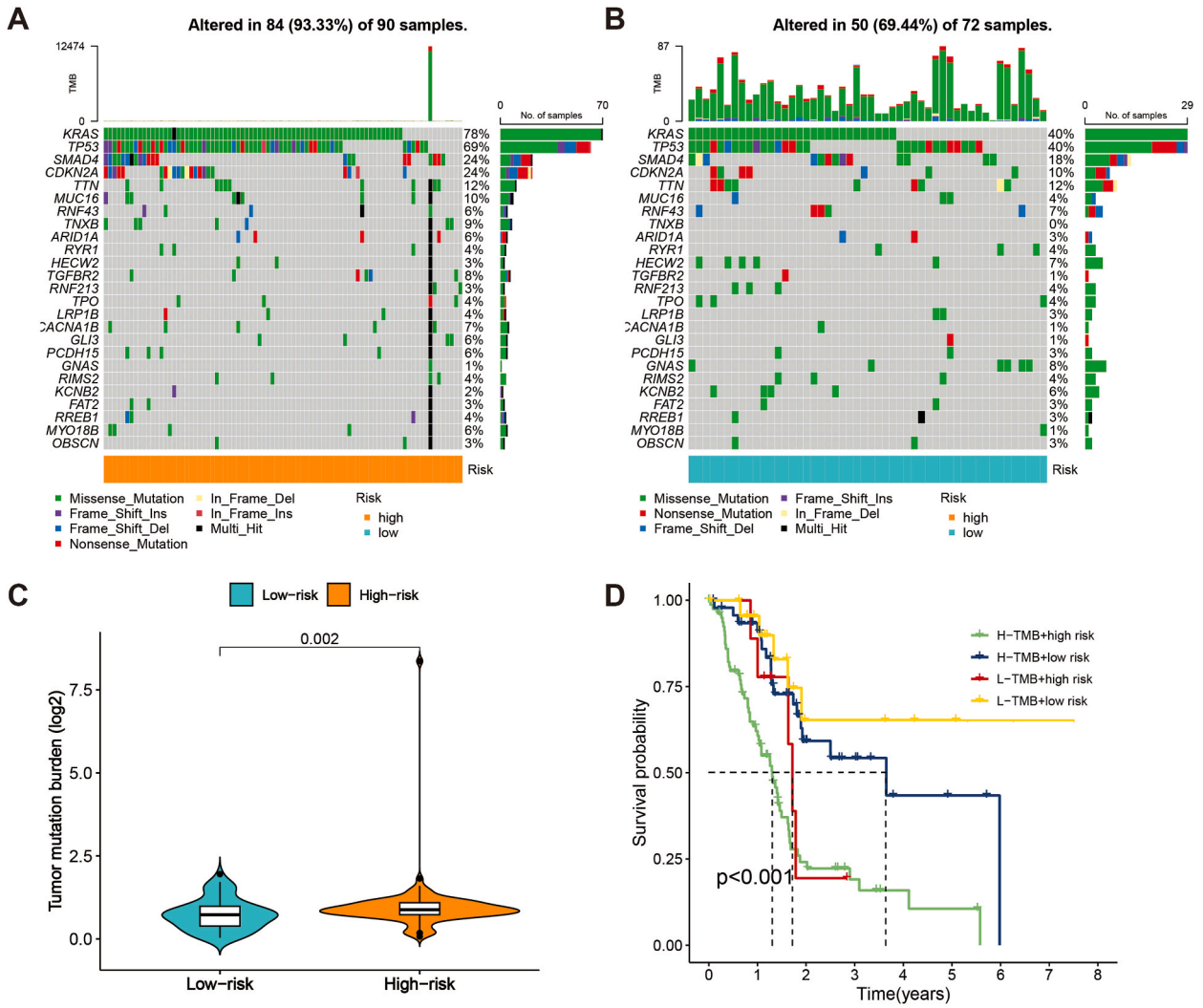

Fig. 8. Correlation of the sphingolipid metabolism-related signature with somatic mutation analysis. (A–B) Mutation waterfall plot of the 25 most frequently mutated genes in the high- and low-risk groups. **(C)** Violin plot of TMB status in the high- and low-risk subgroups. **(D)** Kaplan–Meier curves for TMB subgroups and risk subgroups combined with each other.

(Fig. 12G).

4. Discussion

As a major component of the cell membrane, altered levels of sphingolipid metabolism can directly affect the composition of the cell membrane through the capture of sphingolipids and their metabolites in the lysosome. Abnormalities in sphingolipid metabolism can lead to alterations in lipid homeostasis and are closely associated with various diseases [42,43]. Recently, the relationship between sphingolipid metabolism and tumors has gained traction. As biological effectors, sphingolipids not only regulate malignant biological behaviors such as apoptosis, proliferation and migration of tumor cells but are also associated with tumor immunity and tumor drug resistance [10,44,45]. A previous mass spectrometry-based lipidomics study quantified the changes in sphingolipid-like lipids in pancreatic tumors and plasma specimens and reported that sphingolipid metabolism was altered in human pancreatic cancer and correlated with the advanced stage of the tumor [46]. A recently reported study systematically analyzed glycosphingolipids isolated from pancreatic cancer tissues, which revealed differences in the profiles and relative amounts of neutral glycosphingolipids between normal and tumor tissues [47]. Additionally, it has been demonstrated that sphingolipids are engaged in the regulation of tumorigenesis and metastasis in pancreatic cancer [12,48]. Therefore, the interaction between sphingolipid metabolism and pancreatic cancer along with the potential value of sphingolipid metabolism in predicting the clinical outcomes and therapeutic efficacy of patients with pancreatic cancer are worth exploring.

Recent studies report that lncRNAs are potential targets for tumor therapy and can broadly regulate the progression, metastasis,

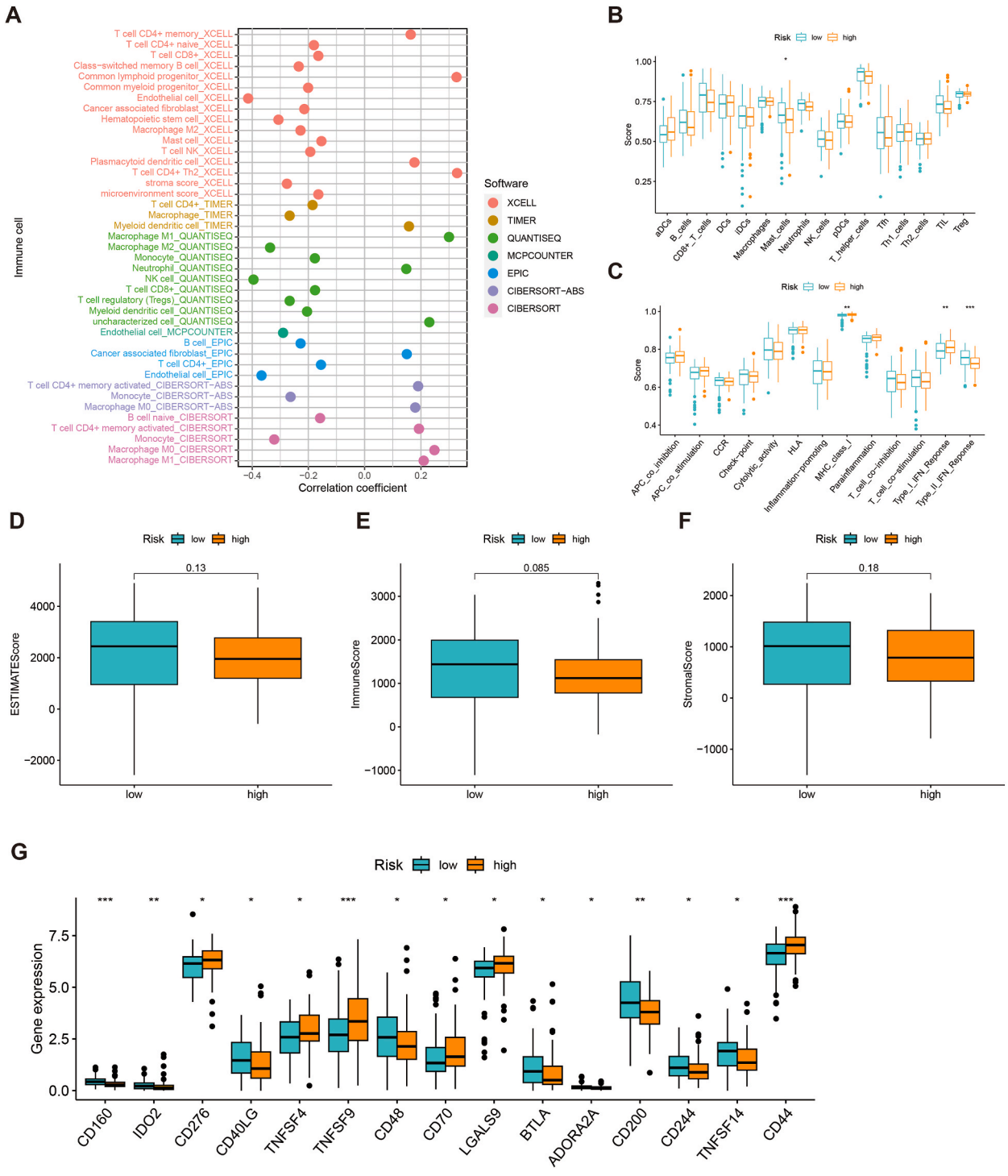

Fig. 9. Correlation of the sphingolipid metabolism-related signature with the immune microenvironment. (A) Bubble plots reveal the relationship between risk scores and immune cell infiltration. **(B)** Box plots show the differences in the degree of different immune cell infiltration based on ssGSEA between risk subgroups. **(C)** Box plots show the differences in different immune functions between the risk subgroups based on ssGSEA. **(D–F)** Box plot showing the relationship between ESTIMATE, immune and stromal scores across the risk subgroups. **(G)** Box plot showing immune checkpoints with significant differences in expression between the risk subgroups.

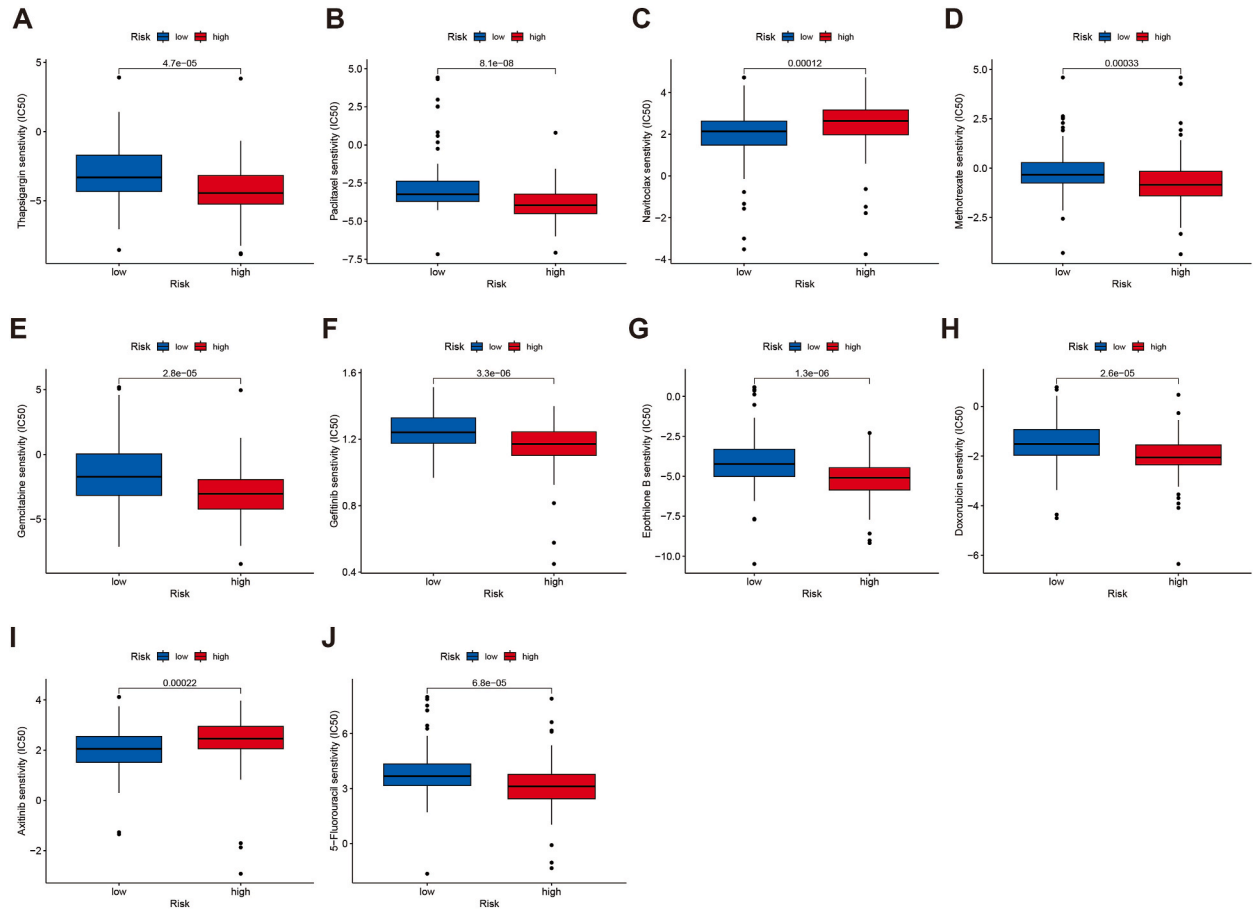

Fig. 10. Drug sensitivity analysis of the risk subgroups. (A) Thapsigargin. **(B)** Paclitaxel. **(C)** Navitoclax. **(D)** Methotrexate. **(E)** Gemcitabine. **(F)** Gefitinib. **(G)** Epothilone B. **(H)** Doxorubicin. **(I)** Axitinib. **(J)** 5-Fluorouracil.

drug resistance and other malignant biological behavior of pancreatic cancer [49–51]. Although the value of lncRNAs as prognostic and efficacy determinants is currently not widely used in practical clinical settings, several studies have demonstrated that circulating lncRNAs are stably present in plasma, serum, and urine, and can be used as noninvasive biomarkers for a variety of tumors [52,53]. A group of lncRNAs with procancer effects have been identified as novel markers and potential targets for intervention in pancreatic cancer [54]. Additionally, lncRNAs also play a regulatory role in a variety of metabolic processes [55,56]. However, the role of sphingolipid metabolism-related lncRNAs in pancreatic cancer is unclear. Therefore, identifying sphingolipid metabolism-related lncRNAs and exploring their potential roles in pancreatic cancer could provide innovative ideas for the advancement of diagnostic and therapeutic strategies.

In the current study, we developed a signature (SMLs) based on sphingolipid metabolism-associated lncRNAs to predict clinical outcomes in individuals with PAAD. Patients in the TCGA-PAAD cohort were divided into high- and low-risk groups according to the risk scores of the SMLs, and the predictive stability of the SMLs was validated in the training and testing sets. The predictive efficacy of the SMLs was also assessed using uni- and multi-Cox regression, ROC curves and clinical subtype stratification analysis, which revealed high stability and excellent prognostic predictive capability. Among the seven lncRNAs comprising the SMLs, MEG9 was speculated to be associated with m6A and affect the clinical outcomes of individuals with PAAD [57]. Moreover, LINC00519 was speculated to be a pyroptosis-associated lncRNA in PAAD and a risk factor for patient survival [58]. However, AC068580.2, LINC02528, PTPRN2-AS1, AC007292.2 and CH17-340M24.3 remain unreported in PAAD. Given the prognostic value of the SMLs in PAAD, the regulatory mechanisms of these lncRNAs in PAAD deserve further exploration.

Somatic mutations in the *KRAS, TP53, SMAD4* and *CDKN2A* genes are considered molecular genetic characteristics and primary drivers of the vast majority of patients with PAAD [59]. Among them, mutations in *KRAS*, the most frequently mutated gene in PAAD, affect the ability of T cells to recognize tumor cells and inhibit tumor killing by effector immune cells [60]. Furthermore, *TP53* is an oncogene with the highest relevance to human tumorigenesis to date. It has the second highest mutation frequency in PAAD and promotes immune evasion by inhibiting T-cell recruitment [61]. In the present study, *KRAS* and *TP53* were mutated much more frequently in the high-risk population, which partly explains the poorer prognosis in the high-risk population compared to the low-risk population. Furthermore, our findings also revealed that the TMB was higher in the high-risk population. Notably, the combination of

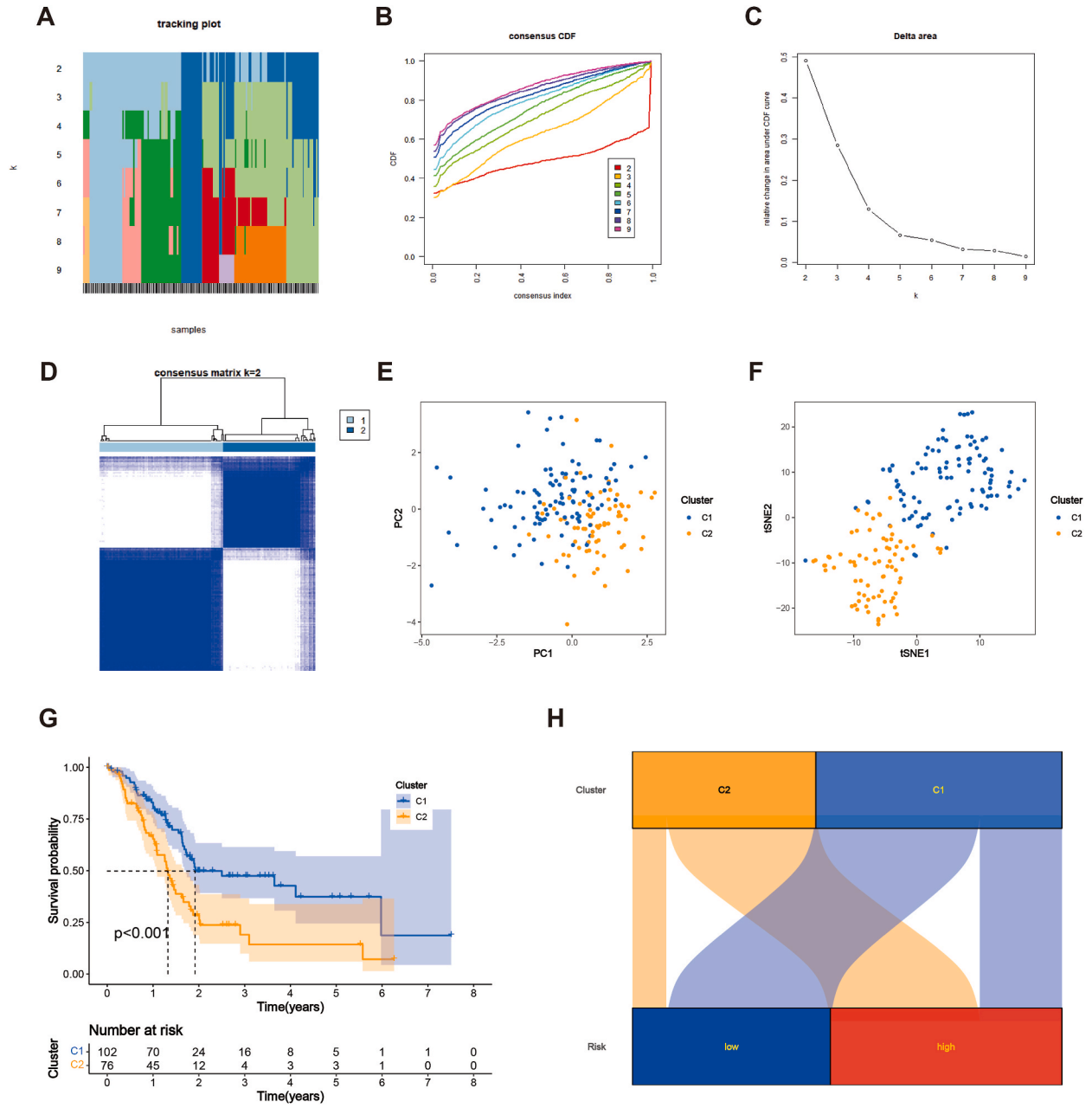

Fig. 11. Consensus clustering analysis of patients with PAAD using the sphingolipid metabolism-related signature. (A–C) Consensus clustering modules with cumulative distribution features by k from 2 to 9. **(D)** The TCGA-PAAD cohort was classified into two clusters based on the consensus clustering matrix. **(E–F)** PCA and tSNE show the distribution characteristics of the two clusters. **(G)** K–M curve showing the difference in survival between the two clusters. **(H)** Sankey diagram showing the relationship between the two clusters and risk subgroups.

TMB levels and risk status allows for a more precise prognostic stratification of patients with PAAD.

The early stage of pancreatic cancer is not clinically obvious. Additionally, most patients are already at an advanced stage by the time they are diagnosed, so the opportunity for surgery is missed [62]. Moreover, the remarkable metastatic capacity and drug resistance of PAAD also lead to a poor prognosis for patients [63,64]. Therefore, it is essential to identify biomarkers that predict the efficacy of PAAD treatment and can contribute to the personalization of treatment regimens for patients, thereby improving clinical outcomes. Currently, the treatment of clinically advanced pancreatic cancer mainly consists of chemotherapy, with gemcitabine and 5-fluorouracil being the cornerstone drugs. Both of these drugs are used as first and second lines treatments to each other. In the present study, the IC50 values for both gemcitabine and 5-fluorouracil were significantly lower in the high-risk population, suggesting that the high-risk population is more likely to benefit from them. Notably, the same results were observed with certain

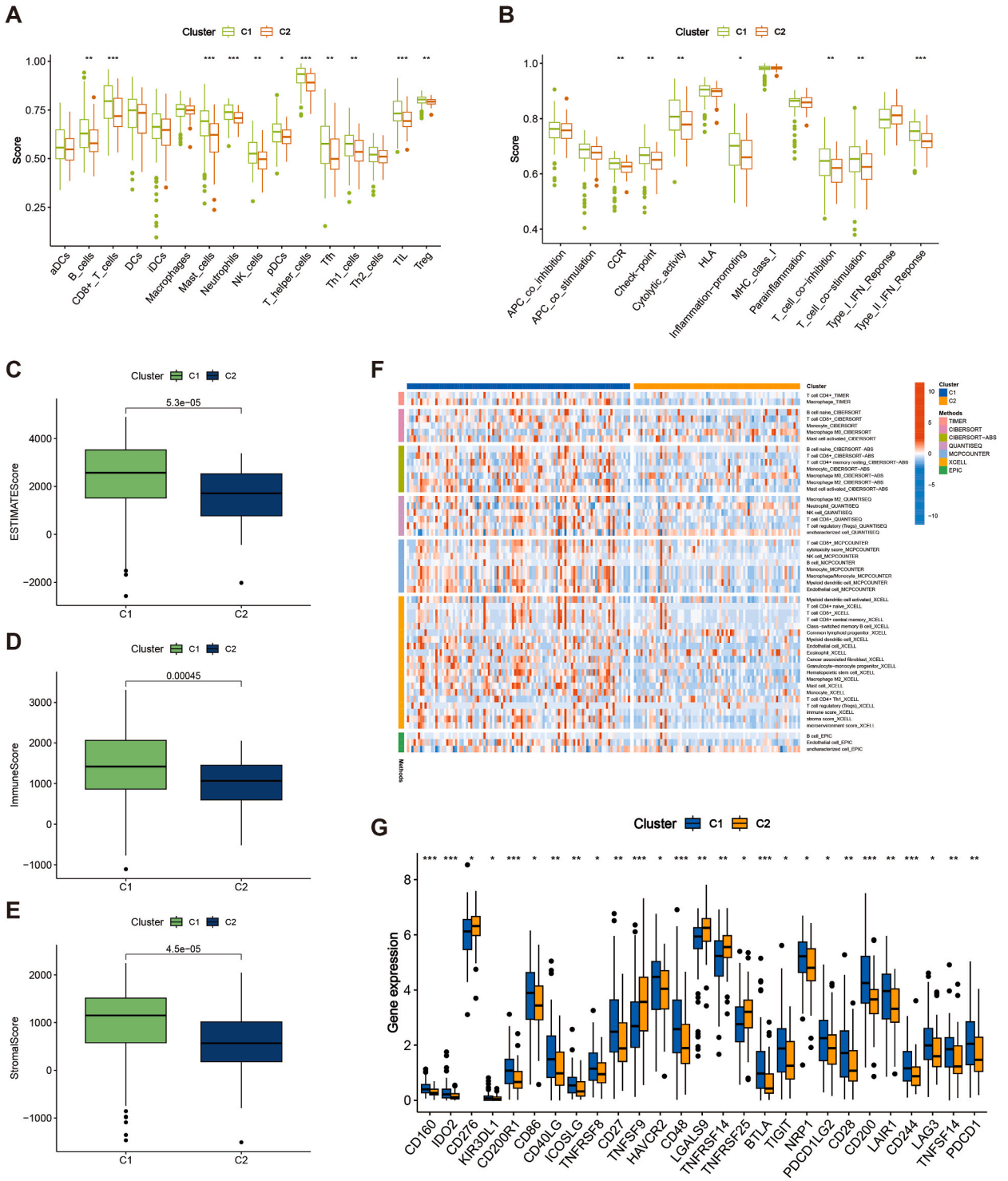

Fig. 12. Consensus clustering analysis to characterize the immune microenvironment. (A) Box plots show the differences in the degree of different immune cell infiltration based on ssGSEA between the two clusters. **(B)** Box plots showing differences in different immune functions in the two clusters based on ssGSEA. **(C–E)** Box plot showing the relationship among ESTIMATE, immune and stromal scores across the different clusters. **(F)** Heatmap showing differences in immune cell infiltration between the different clusters. **(G)** Box plot showing immune checkpoints with significant differences in expression between the different clusters.

chemotherapeutic agents, namely paclitaxel, methotrexate, epothilone B and doxorubicin, suggesting that high-risk individuals have superior response rates to chemotherapeutic agents. Additionally, the Bcl-2/Bcl-xL inhibitor navitoclax induced apoptosis in pancreatic cancer cells, thereby enhancing the antitumour efficacy of checkpoint kinase 1 inhibitors [65]. Nonetheless, the low-risk groups were found to be more likely to benefit from navitoclax. Moreover, these results were also observed with axitinib, a selective vascular endothelial growth factor receptor-targeting drug. Overall, the findings suggest that risk stratification based on the SMLs could provide a basis for individualized clinical planning of chemotherapeutic agents and targeted drugs.

Although risk stratification based on the SMLs can better predict the survival and clinical outcomes of patients with PAAD, it cannot distinguish populations with different TIME characteristics. Studies have shown that tumor subgroups derived from consensus clustering analysis have different TIME characteristics and impact immunotherapy response [66–68]. Accordingly, we performed a consensus clustering analysis based on the constructed SMLs, dividing the TCGA-PAAD cohort into two clusters to further explore the differences in clinical outcomes and the TIME of patients in different subtypes. The results showed significantly better survival in Cluster 1 than in Cluster 2. Furthermore, ssGSEA also revealed significantly higher levels of infiltration of most immune cells, including $CD8^+$ T cells, neutrophils and natural killer cells, in Cluster 1 than in Cluster 2, which was also validated by ssGSEA immune function analysis, TIMER2.0 platform analysis and ESTIMATE analysis. Thus, these results suggest a high immune infiltration status in Cluster 1, which could partly explain the better prognosis of Cluster 1. Overall, cluster analysis based on the SMLs not only predicts the clinical outcomes of patients with PAAD but also better differentiates between populations with different TIME characteristics.

Over the past decade, ICIs have received increasing attention for their significant antitumour effects, which offer new hope for patients with cancer. ICIs reactivate the antitumour activity of T lymphocytes by inhibiting the interaction between immune checkpoints, thereby achieving antitumour effects [69]. However, identifying the population that will benefit from ICIs is a challenging aspect of clinical treatment. Previous research has confirmed that tumors defined by high infiltration of effector immune cells such as $CD8^+$ T cells and immune checkpoint activation are immune 'hot tumors', which may respond better to treatment with ICIs [69,70]. In this study, in Cluster 1, most immune checkpoints, including PD-1, LAG3, CD27 and CD48, were highly expressed and also exhibited a high immune infiltration status. Thus, Cluster 1 is more consistent with the immune 'hot tumor' subgroup, suggesting that Cluster 1 may respond better to ICI treatment. Therefore, the SMLs-based consensus clustering analysis not only predicts patient prognosis and TIME profiles but also helps to identify the population that will benefit from treatment with ICIs.

Although the SLMs developed in this study were validated and evaluated by different methodologies, there are still some limitations. First, it was not possible to assess the bias of the data in a retrospective study. Additionally, the application of lncRNAs as biomarkers in the clinical real world has not yet been popularized, and their potential predictive value and applicability still need to be further confirmed in future clinical studies with large sample sizes. Thus, this is also an important direction for our future research extension.

5. Conclusion

To the best of our knowledge, this is the first signature in PAAD that was constructed based on sphingolipid metabolism-related lncRNAs. The SMLs effectively predicts clinical outcomes in patients with PAAD and serves as a basis for personalized therapeutic regimen selection for certain clinical chemotherapeutic agents and targeted drugs. Furthermore, SMLs-based cluster differentiation not only predicts patient prognosis but also helps to differentiate patients with different TIME profiles, identify immune 'hot tumors' and determine the potential beneficiary population for treatment with ICIs.

Data availability statement

Data included in article/supp. material/referenced in article.

Funding sources

This work was funded by the Project of NINGBO Leading Medical & Health Discipline, Project Number: 2022-X07.

CRediT authorship contribution statement

Xiaolan He: Writing – review & editing, Funding acquisition, Data curation, Conceptualization. **Zhengyang Xu:** Writing – review & editing, Supervision. **Ruiping Ren:** Data curation. **Peng Wan:** Writing – original draft, Software. **Yu Zhang:** Methodology, Data curation. **Liangliang Wang:** Visualization, Supervision. **Ying Han:** Supervision, Investigation.

Declaration of competing interest

The authors declare that they have no known competing financial interests or personal relationships that could have appeared to influence the work reported in this paper.

Acknowledgments

We thank Bullet Edits Limited for the linguistic editing and proofreading of the manuscript.

Appendix A. Supplementary data

Supplementary data to this article can be found online at https://doi.org/10.1016/j.heliyon.2023.e23659.

References

[1] H. Sung, J. Ferlay, R.L. Siegel, M. Laversanne, I. Soerjomataram, A. Jemal, F. Bray, Global cancer statistics 2020: GLOBOCAN estimates of incidence and mortality worldwide for 36 cancers in 185 countries, CA: a cancer journal for clinicians 71 (2021) 209–249.
[2] R.L. Siegel, K.D. Miller, H.E. Fuchs, A. Jemal, Cancer statistics, 2022, CA: a cancer journal for clinicians 72 (2022) 7–33.
[3] J. Huang, V. Lok, C.H. Ngai, L. Zhang, J. Yuan, X.Q. Lao, K. Ng, C. Chong, Z.J. Zheng, M.C.S. Wong, Worldwide burden of, risk factors for, and trends in pancreatic cancer, Gastroenterology 160 (2021) 744–754.
[4] J. Ferlay, C. Partensky, F. Bray, More deaths from pancreatic cancer than breast cancer in the EU by 2017, Acta oncologica (Stockholm, Sweden) 55 (2016) 1158–1160.
[5] Y.A. Hannun, L.M. Obeid, Principles of bioactive lipid signalling: lessons from sphingolipids, Nat. Rev. Mol. Cell Biol. 9 (2008) 139–150.
[6] M.L. Kraft, Sphingolipid organization in the plasma membrane and the mechanisms that influence it, Front. Cell Dev. Biol. 4 (2016) 154.
[7] M. Ivanova, Altered sphingolipids metabolism damaged mitochondrial functions: lessons learned from gaucher and fabry diseases, J. Clin. Med. 9 (2020).
[8] L.B. Fugio, F.B. Coeli-Lacchini, A.M. Leopoldino, Sphingolipids and mitochondrial dynamic, Cells (2020) 9.
[9] H. Tang, X. Huang, S. Pang, Regulation of the lysosome by sphingolipids: potential role in aging, J. Biol. Chem. 298 (2022), 102118.
[10] B. Ogretmen, Sphingolipid metabolism in cancer signalling and therapy, Nat. Rev. Cancer 18 (2018) 33–50.
[11] S.H. Patel, M. Bachmann, S. Kadow, G.C. Wilson, M.M.L. Abdel-Salam, K. Xu, S. Keitsch, M. Soddemann, B. Wilker, K.A. Becker, A. Carpinteiro, S.A. Ahmad, I. Szabo, et al., Simultaneous targeting of mitochondrial Kv1.3 and lysosomal acid sphingomyelinase amplifies killing of pancreatic ductal adenocarcinoma cells in vitro and in vivo, J. Mol. Med. (Berl). 101 (3) (2023) 295–310.
[12] Y. Zhang, S. Ji, X. Zhang, M. Lu, Y. Hu, Y. Han, G. Shui, S.M. Lam, X. Zou, Human CPTP promotes growth and metastasis via sphingolipid metabolite ceramide and PI4KA/AKT signaling in pancreatic cancer cells, Int. J. Biol. Sci. 18 (2022) 4963–4983.
[13] M.P. Dragomir, S. Kopetz, J.A. Ajani, G.A. Calin, Non-coding RNAs in GI cancers: from cancer hallmarks to clinical utility, Gut 69 (2020) 748–763.
[14] J. Zhao, P. Du, P. Cui, Y. Qin, C. Hu, J. Wu, Z. Zhou, W. Zhang, L. Qin, G. Huang, LncRNA PVT1 promotes angiogenesis via activating the STAT3/VEGFA axis in gastric cancer, Oncogene 37 (2018) 4094–4109.
[15] M. Sun, W.L. Kraus, From discovery to function: the expanding roles of long noncoding RNAs in physiology and disease, Endocr. Rev. 36 (2015) 25–64.
[16] A. Fatica, I. Bozzoni, Long non-coding RNAs: new players in cell differentiation and development, Nat. Rev. Genet. 15 (2014) 7–21.
[17] J.A. Peña-Flores, D. Enríquez-Espinoza, D. Muela-Campos, A. Álvarez-Ramírez, A. Sáenz, A.A. Barraza-Gómez, K. Bravo, M.E. Estrada-Macías, K. González-Alvarado, Functional relevance of the long intergenic non-coding RNA regulator of reprogramming (Linc-ROR) in cancer proliferation, metastasis, and drug resistance, Non-coding RNA 9 (2023).
[18] S. Zheng, W. Fu, Q. Huang, J. Zhou, K. Lu, J. Gu, R. Ma, G. Guo, LncRNA PRKCQ-AS1 regulates paclitaxel resistance in triple-negative breast cancer cells through miR-361-5p/PIK3C3 mediated autophagy, Clinical and experimental pharmacology & physiology (2023).
[19] X. Wang, Y. Xu, X. Wang, C. Jiang, S. Han, K. Dong, M. Shen, D. Xu, LincRNA-p21 suppresses development of human prostate cancer through inhibition of PKM2, Cell Prolif. 50 (2017).
[20] J. Li, P. Song, T. Jiang, D. Dai, H. Wang, J. Sun, L. Zhu, W. Xu, L. Feng, V.Y. Shin, H. Morrison, X. Wang, H. Jin, Heat shock factor 1 epigenetically stimulates glutaminase-1-dependent mTOR activation to promote colorectal carcinogenesis, Mol. Ther. : the journal of the American Society of Gene Therapy 26 (2018) 1828–1839.
[21] M. Cui, Z. Xiao, Y. Wang, M. Zheng, T. Song, X. Cai, B. Sun, L. Ye, X. Zhang, Long noncoding RNA HULC modulates abnormal lipid metabolism in hepatoma cells through an miR-9-mediated RXRA signaling pathway, Cancer Res. 75 (2015) 846–857.
[22] W. Lin, Q. Zhou, C.Q. Wang, L. Zhu, C. Bi, S. Zhang, X. Wang, H. Jin, LncRNAs regulate metabolism in cancer, Int. J. Biol. Sci. 16 (2020) 1194–1206.
[23] Y. Ye, Q. Zhao, Y. Wu, G. Wang, Y. Huang, W. Sun, M. Zhang, Construction of a cancer-associated fibroblasts-related long non-coding RNA signature to predict prognosis and immune landscape in pancreatic adenocarcinoma, Front. Genet. 13 (2022), 989719.
[24] H. Chi, G. Peng, J. Yang, J. Zhang, G. Song, X. Xie, D.F. Strohmer, G. Lai, S. Zhao, R. Wang, F. Yang, G. Tian, Machine learning to construct sphingolipid metabolism genes signature to characterize the immune landscape and prognosis of patients with uveal melanoma, Front. Endocrinol. 13 (2022), 1056310.
[25] K. Breuer, A.K. Foroushani, M.R. Laird, C. Chen, A. Sribnaia, R. Lo, G.L. Winsor, R.E. Hancock, F.S. Brinkman, D.J. Lynn, InnateDB: systems biology of innate immunity and beyond–recent updates and continuing curation, Nucleic acids research 41 (2013) D1228–D1233.
[26] M.E. Ritchie, B. Phipson, D. Wu, Y. Hu, C.W. Law, W. Shi, G.K. Smyth, Limma powers differential expression analyses for RNA-sequencing and microarray studies, Nucleic acids research 43 (2015) e47.
[27] J. Ren, A. Wang, J. Liu, Q. Yuan, Identification and validation of a novel redox-related lncRNA prognostic signature in lung adenocarcinoma, Bioengineered 12 (2021) 4331–4348.
[28] Q. Yuan, J. Ren, L. Li, S. Li, K. Xiang, D. Shang, Development and validation of a novel N6-methyladenosine (m6A)-related multi- long non-coding RNA (lncRNA) prognostic signature in pancreatic adenocarcinoma, Bioengineered 12 (2021) 2432–2448.
[29] Q. Yuan, W. Zhang, W. Shang, Identification and validation of a prognostic risk-scoring model based on sphingolipid metabolism-associated cluster in colon adenocarcinoma, Front. Endocrinol. 13 (2022), 1045167.
[30] Z. Gu, R. Eils, M. Schlesner, Complex heatmaps reveal patterns and correlations in multidimensional genomic data, Bioinformatics 32 (2016) 2847–2849.
[31] S. Hänzelmann, R. Castelo, J. Guinney, GSVA: gene set variation analysis for microarray and RNA-seq data, BMC Bioinf. 14 (2013) 7.
[32] V. Anagnostou, A. Bardelli, T.A. Chan, S. Turajlic, The status of tumor mutational burden and immunotherapy, Nature cancer 3 (2022) 652–656.
[33] T. Li, J. Fu, Z. Zeng, D. Cohen, J. Li, Q. Chen, B. Li, X.S. Liu, TIMER2.0 for analysis of tumor-infiltrating immune cells, Nucleic acids research 48 (2020) W509–w514.
[34] A. Subramanian, P. Tamayo, V.K. Mootha, S. Mukherjee, B.L. Ebert, M.A. Gillette, A. Paulovich, S.L. Pomeroy, T.R. Golub, E.S. Lander, J.P. Mesirov, Gene set enrichment analysis: a knowledge-based approach for interpreting genome-wide expression profiles, Proc. Natl. Acad. Sci. U.S.A. 102 (2005) 15545–15550.
[35] D.A. Barbie, P. Tamayo, J.S. Boehm, S.Y. Kim, S.E. Moody, I.F. Dunn, A.C. Schinzel, P. Sandy, E. Meylan, C. Scholl, S. Fröhling, E.M. Chan, M.L. Sos, K. Michel, C. Mermel, S.J. Silver, B.A. Weir, J.H. Reiling, Q. Sheng, P.B. Gupta, R.C. Wadlow, H. Le, S. Hoersch, B.S. Wittner, S. Ramaswamy, D.M. Livingston, D. M. Sabatini, M. Meyerson, R.K. Thomas, E.S. Lander, J.P. Mesirov, D.E. Root, D.G. Gilliland, T. Jacks, W.C. Hahn, Systematic RNA interference reveals that oncogenic KRAS-driven cancers require TBK1, Nature 462 (2009) 108–112.
[36] K. Yoshihara, M. Shahmoradgoli, E. Martínez, R. Vegesna, H. Kim, W. Torres-Garcia, V. Treviño, H. Shen, P.W. Laird, D.A. Levine, S.L. Carter, G. Getz, K. Stemke-Hale, G.B. Mills, R.G. Verhaak, Inferring tumour purity and stromal and immune cell admixture from expression data, Nat. Commun. 4 (2013) 2612.
[37] Y. Zhang, J. Zheng, Functions of immune checkpoint molecules beyond immune evasion, Adv. Exp. Med. Biol. 1248 (2020) 201–226.
[38] P. Geeleher, N. Cox, R.S. Huang, pRRophetic: an R package for prediction of clinical chemotherapeutic response from tumor gene expression levels, PLoS One 9 (2014), e107468.
[39] W. Wang, Y. Ye, X. Zhang, W. Sun, L. Bao, An angiogenesis-related three-long non-coding ribonucleic acid signature predicts the immune landscape and prognosis in hepatocellular carcinoma, Heliyon 9 (2023), e13989.

[40] W. Wang, Y. Ye, X. Zhang, X. Ye, C. Liu, L. Bao, Construction of a necroptosis-associated long non-coding RNA signature to predict prognosis and immune response in hepatocellular carcinoma, Front. Mol. Biosci. 9 (2022), 937979.
[41] M.D. Wilkerson, D.N. Hayes, ConsensusClusterPlus: a class discovery tool with confidence assessments and item tracking, Bioinformatics 26 (2010) 1572–1573.
[42] M. Abed Rabbo, Y. Khodour, L.S. Kaguni, J. Stiban, Sphingolipid lysosomal storage diseases: from bench to bedside, Lipids Health Dis. 20 (2021) 44.
[43] F. Parveen, D. Bender, S.H. Law, V.K. Mishra, C.C. Chen, L.Y. Ke, Role of ceramidases in sphingolipid metabolism and human diseases, Cells (2019) 8.
[44] R.Z. Li, X.R. Wang, J. Wang, C. Xie, X.X. Wang, H.D. Pan, W.Y. Meng, T.L. Liang, J.X. Li, P.Y. Yan, Q.B. Wu, L. Liu, X.J. Yao, E.L. Leung, The key role of sphingolipid metabolism in cancer: new therapeutic targets, diagnostic and prognostic values, and anti-tumor immunotherapy resistance, Front. Oncol. 12 (2022), 941643.
[45] S. Vaena, P. Chakraborty, H.G. Lee, A.H. Janneh, M.F. Kassir, G. Beeson, Z. Hedley, A. Yalcinkaya, M.H. Sofi, H. Li, M.L. Husby, R.V. Stahelin, X.Z. Yu, S. Mehrotra, B. Ogretmen, Aging-dependent mitochondrial dysfunction mediated by ceramide signaling inhibits antitumor T cell response, Cell Rep. 35 (2021), 109076.
[46] Y. Jiang, N.A. DiVittore, M.M. Young, Z. Jia, K. Xie, T.M. Ritty, M. Kester, T.E. Fox, Altered sphingolipid metabolism in patients with metastatic pancreatic cancer, Biomolecules 3 (2013) 435–448.
[47] K. Hořejší, C. Jin, Z. Vaňková, R. Jirásko, O. Strouhal, B. Melichar, S. Teneberg, M. Holčapek, Comprehensive characterization of complex glycosphingolipids in human pancreatic cancer tissues, J. Biol. Chem. 299 (2023), 102923.
[48] D. Qi, X. Song, C. Xue, W. Yao, P. Shen, H. Yu, Z. Zhang, AKT1/FOXP3 axis-mediated expression of CerS6 promotes p53 mutant pancreatic tumorigenesis, Cancer letters 522 (2021) 105–118.
[49] F. Xu, M. Huang, Q. Chen, Y. Niu, Y. Hu, P. Hu, D. Chen, C. He, K. Huang, Z. Zeng, J. Tang, F. Wang, Y. Zhao, C. Wang, G. Zhao, LncRNA HIF1A-AS1 promotes gemcitabine resistance of pancreatic cancer by enhancing glycolysis through modulating the AKT/YB1/HIF1α pathway, Cancer Res. 81 (2021) 5678–5691.
[50] H. Zhang, C. Zhu, Z. He, S. Chen, L. Li, C. Sun, LncRNA PSMB8-AS1 contributes to pancreatic cancer progression via modulating miR-382-3p/STAT1/PD-L1 axis, J. Exp. Clin. Cancer Res. : CR 39 (2020) 179.
[51] L.F. Sempere, K. Powell, J. Rana, A.A. Brock, T.D. Schmittgen, Role of non-coding RNAs in tumor progression and metastasis in pancreatic cancer, Cancer Metastasis Rev. 40 (2021) 761–776.
[52] L.Y. Lin, L. Yang, Q. Zeng, L. Wang, M.L. Chen, Z.H. Zhao, G.D. Ye, Q.C. Luo, P.Y. Lv, Q.W. Guo, B.A. Li, J.C. Cai, W.Y. Cai, Tumor-originated exosomal lncUEGC1 as a circulating biomarker for early-stage gastric cancer, Mol. Cancer 17 (2018) 84.
[53] P. Qi, X.Y. Zhou, X. Du, Circulating long non-coding RNAs in cancer: current status and future perspectives, Mol. Cancer 15 (2016) 39.
[54] V.F. da Paixão, O.J. Sosa, D.V. da Silva Pellegrina, B. Dazzani, T.B. Corrêa, E. Risério Bertoldi, E.A.-d.-M.L.B. da Cruz, D. de Oliveira Pessoa, V. de Paiva Oliveira, R. Alberto Chiong Zevallos, L.C. Russo, F.L. Forti, J. Eduardo Ferreira, H. Carioca Freitas, J. Jukemura, M.C.C. Machado, M. Dirlei Begnami, J.C. Setubal, D. S. Bassères, E. Moraes Reis, Annotation and functional characterization of long noncoding RNAs deregulated in pancreatic adenocarcinoma, Cell. Oncol. (Dordrecht) 45 (2022) 479–504.
[55] J. He, F. Li, Y. Zhou, X. Hou, S. Liu, X. Li, Y. Zhang, X. Jing, L. Yang, LncRNA XLOC_006390 promotes pancreatic carcinogenesis and glutamate metabolism by stabilizing c-Myc, Cancer letters 469 (2020) 419–428.
[56] Y. Ma, M. Hu, L. Zhou, S. Ling, Y. Li, B. Kong, P. Huang, Long non-coding RNA HOTAIR promotes cancer cell energy metabolism in pancreatic adenocarcinoma by upregulating hexokinase-2, Oncol. Lett. 18 (2019) 2212–2219.
[57] P.W. Cao, L. Liu, Z.H. Li, F. Cao, F.B. Liu, Prognostic value of drug targets predicted using deep bioinformatic analysis of m6A-associated lncRNA-based pancreatic cancer model characteristics and its tumour microenvironment, Front. Genet. 13 (2022), 853471.
[58] K. Zhao, X. Li, Y. Shi, Y. Lu, P. Qiu, Z. Deng, W. Yao, J. Wang, A comprehensive analysis of pyroptosis-related lncRNAs signature associated with prognosis and tumor immune microenvironment of pancreatic adenocarcinoma, Front. Genet. 13 (2022), 899496.
[59] L. Cao, C. Huang, D. Cui Zhou, Y. Hu, T.M. Lih, S.R. Savage, K. Krug, D.J. Clark, M. Schnaubelt, L. Chen, F. da Veiga Leprevost, R.V. Eguez, W. Yang, J. Pan, B. Wen, Y. Dou, W. Jiang, Y. Liao, Z. Shi, N.V. Terekhanova, S. Cao, R.J. Lu, Y. Li, R. Liu, H. Zhu, P. Ronning, Y. Wu, M.A. Wyczalkowski, H. Easwaran, L. Danilova, A.S. Mer, S. Yoo, J.M. Wang, W. Liu, B. Haibe-Kains, M. Thiagarajan, S.D. Jewell, G. Hostetter, C.J. Newton, Q.K. Li, M.H. Roehrl, D. Fenyö, P. Wang, A.I. Nesvizhskii, D.R. Mani, G.S. Omenn, E.S. Boja, M. Mesri, A.I. Robles, H. Rodriguez, O.F. Bathe, D.W. Chan, R.H. Hruban, L. Ding, B. Zhang, H. Zhang, Proteogenomic characterization of pancreatic ductal adenocarcinoma, Cell 184 (2021), e5026, 5031-5052.
[60] J. Cullis, S. Das, D. Bar-Sagi, Kras and tumor immunity: friend or foe? Cold Spring Harbor perspectives in medicine 8 (2018).
[61] J. Blagih, M.D. Buck, K.H. Vousden, p53, cancer and the immune response, J. Cell Sci. 133 (2020).
[62] J. Kleeff, M. Korc, M. Apte, C. La Vecchia, C.D. Johnson, A.V. Biankin, R.E. Neale, M. Tempero, D.A. Tuveson, R.H. Hruban, J.P. Neoptolemos, Pancreatic cancer, Nature reviews, Disease primers 2 (2016), 16022.
[63] K. Masuo, R. Chen, A. Yogo, A. Sugiyama, A. Fukuda, T. Masui, S. Uemoto, H. Seno, S. Takaishi, SNAIL2 contributes to tumorigenicity and chemotherapy resistance in pancreatic cancer by regulating IGFBP2, Cancer Sci. 112 (2021) 4987–4999.
[64] X. Xin, V. Kumar, F. Lin, V. Kumar, R. Bhattarai, V.R. Bhatt, C. Tan, R.I. Mahato, Redox-responsive nanoplatform for codelivery of miR-519c and gemcitabine for pancreatic cancer therapy, Sci. Adv. 6 (2020).
[65] Y. Morimoto, K. Takada, O. Takeuchi, K. Watanabe, M. Hirohara, T. Hamamoto, Y. Masuda, Bcl-2/Bcl-xL inhibitor navitoclax increases the antitumor effect of Chk1 inhibitor prexasertib by inducing apoptosis in pancreatic cancer cells via inhibition of Bcl-xL but not Bcl-2, Mol. Cell. Biochem. 472 (2020) 187–198.
[66] X. Wang, L. Chen, H. Cao, J. Huang, Identification of gene signature-related oxidative stress for predicting prognosis of colorectal cancer, Oxid. Med. Cell. Longev. 2023 (2023), 5385742.
[67] J. Li, C. Yang, Y. Zheng, Identification of a tissue resident memory CD8 T cell-related risk score signature for colorectal cancer, the association with TME landscapes and therapeutic responses, Front. Genet. 13 (2022), 1088230.
[68] J. Tang, X. Wu, B. Cheng, Y. Lu, Identification of a polyamine-related signature and six novel prognostic biomarkers in oral squamous cell carcinoma, Front. Mol. Biosci. 10 (2023), 1073770.
[69] J. Galon, D. Bruni, Approaches to treat immune hot, altered and cold tumours with combination immunotherapies, Nature reviews, Drug discovery 18 (2019) 197–218.
[70] Y.T. Liu, Z.J. Sun, Turning cold tumors into hot tumors by improving T-cell infiltration, Theranostics 11 (2021) 5365–5386.